ISSN No: 2348-4845
International Journal & Magazine of Engineering, Technology, Management and Research
A Peer Reviewed Open Access International Journal

A High Step-Up Three-Port DC–DC Converter for Stand-Alone PV/Battery Power Systems

Ch.Srinivasulu Reddy, M.Tech
Associate Professor,
PBR Visvodaya Institute of Technology and Science,
Kavali.

S.Amala
M.Tech Student
PBR Visvodaya Institute of Technology and Science,
Kavali.

Abstract:

A three-port dc–dc converter integrating photovoltaic (PV) and battery power for high step-up applications is proposed in this paper. The topology includes five power switches, two coupled inductors, and two active-clamp circuits.

The coupled inductors are used to achieve high step-up voltage gain and to reduce the voltage stress of input side switches. Two sets of active-clamp circuits are used to recycle the energy stored in the leakage inductors and to improve the system efficiency. The operation mode does not need to be changed when a transition between charging and discharging occurs.

Moreover, tracking maximum power point of the PV source and regulating the output voltage can be operated simultaneously during charging/discharging transitions. As long as the sun irradiation level is not too low, the maximum power point tracking (MPPT) algorithm will be disabled only when the battery charging voltage is too high.

Therefore, the control scheme of the proposed converter provides maximum utilization of PV power most of the time. As a result, the proposed converter has merits of high boosting level, reduced number of devices, and simple control strategy. Experimental results of a 200-W laboratory prototype are presented to verify the performance of the proposed three-port converter.

Index Terms:

DC microgrid, energy storage, high step-up application, hybrid power system, renewable energy source, three-port converter.

Introduction:

Integrated multiport converters for interfacing several power sources and storage devices are widely used in recent years. Instead of using individual power electronic converters for each of the energy sources, multiport converters have the advantages including less components, lower cost, more compact size, and better dynamic performance. In many cases, at least one energy storage device should be incorporated. For example, in the electric vehicle application, the regenerative energy occurs during acceleration or startup. Therefore, it is very important for the port connected to the energy storage to allow bidirectional power flow.

In this project, a high step-up three-port dc-dc converter for the hybrid PV/battery system is proposed with the following advantages: 1) high voltage conversion ratio is achieved by using coupled inductors; 2) simple converter topology which has reduced number of the switches and associate circuits; 3) simple control strategy which does not need to change the operation mode after a charging/discharging transition occurs unless the charging voltage is too high; and 4) output voltage is always regulated at 380 V under all operation modes.

It is noted that for the MPP-tracking converters, operating range has to be limited to the voltage less than the MPPT voltage when the output voltage or current control is active [26]. This issue could be addressed by limiting the operating range of the converter in the voltages higher than MPPT. Literature overview DC-DC Converters with High Step-Up Gain High step-up DC-DC converters are widely used to boost the low input voltage level at the front end of distributed power systems.

ISSN No: 2348-4845
International Journal & Magazine of Engineering, Technology, Management and Research
A Peer Reviewed Open Access International Journal

These systems are powered by renewable energy sources such as solar panels, batteries, and fuel cells. The input voltage could range from 12-50 V and the output voltage is typically 380 V. Many non isolated DC-DC converters are proposed [16-32] for high step-up applications. These converters can be roughly divided into several categories: (i) switched capacitor type [16-18]; (ii) coupled inductor type [19-21]; (iii) voltage-lift type [22-24]; (iv) cascaded type[25-27]; (v) isolated-converter-based type[28-32]. High step up gain can be achieved by using switched capacitor technique but there be high transient current on main switch and the conduct loss is high. The converters using coupled inductors could achieve high voltage conversion ratio through adjusting the turn's ratio.

DC-AC Inverters for High Step-Up Applications The DC-AC inverters for high step-up applications can be categorized according to number of power stages and number of high frequency (or low frequency) transformer. In the following, the analysis will focus on the inverters used in PV applications. Inverters for other applications using different renewable sources could utilize similar methodology. A single stage inverter has to do MPPT control and grid current shaping by itself, as shown in Fig 2(a).

This is the typical structure for centralized inverter, with all the drawbacks associated with it. A dual-stage inverter is illustrated in Fig 2(b) and the DC-DC stage is responsible for MPPT (and perhaps voltage amplification). The output of the DC-DC stage could be either pure DC voltage or the output current is modulated to follow the sinusoidal reference. The DC-AC inverter may control the grid current by means of PWM or simply unfold the rectified current to a full sine-wave. It is suggested that the inverter should be operated in PWM mode if the nominal power is high. A solution for multi-string inverter is shown in Fig 2(c). The task for each DC-DC converter is MPPT (and perhaps voltage amplification).

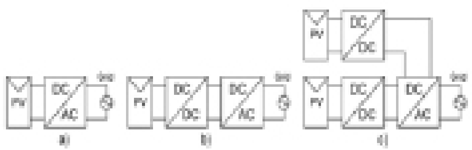

Fig.2.1 Three types of PV inverters (a) single-stage (b) dual-stage (c) dual-stage with paralleled DC-DC stage [6]

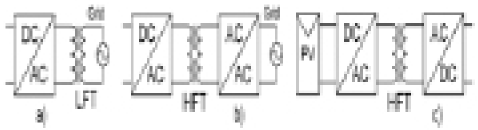

Fig. 2.2 Examples of transformer-included inverter solutions (a) line frequency transformer (LFT) placed between gird and the inverter (b) High-frequency transformer (HFT) imbedded

Topological Modes and Analysis The topology of proposed non-isolated three-port dc-dc converter is illustrated in Fig. 3.The converter is composed of two main switches S1 and S2 for the battery and PV port. Synchronous switch S3 is driven complementarily to S1 such that bidirectional power flow for the battery port can be achieved. Two coupled inductors with winding ratios n1 and n2 are used as voltage gain extension cells. Two sets of active-clamp circuits formed by S4, Lk1, Cc1 and S5, Lk2, Cc2 are used to recycle the leakage energy. Lk1 and Lk2 are both composed of a small leakage inductor from the coupled inductor and an external leakage inductor. Two independent control variables, duty cycles d1 and d2, allow the control over two ports of the converter while the third port is for the power balance. The fixed-frequency driving signals of the auxiliary switches S3 and S4 are complementary to primary switch S1.

Again, S3 provides a bidirectional path for the battery port. Similarly, S5 is driven in a complementary manner to S2. A 180-degree phase-shift is applied between the driving signals of S1 and S2. There are four operation periods based on the available solar power. First, the sun is in the eclipse stage and the solar irradiation is either unavailable or very low. This operation period is defined as period 1, and the battery will serve as the main power source.

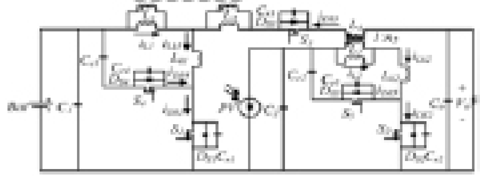

Fig. 3 Topology of the proposed converter.

As the sun starts to shine and the initial solar irradiation is enough for supplying part of the load demand, the operation period is changed to period 2.

ISSN No: 2348-4845
International Journal & Magazine of Engineering, Technology, Management and Research
A Peer Reviewed Open Access International Journal

The load is supplied by both solar and battery power in this period. For period 3, the increasing isolation makes the solar power larger than the load demand. The battery will preserve extra solar power for backup use. During period 4, the charging voltage of the battery reaches the preset level and should be limited to prevent overcharging.

According to the solar irradiation and the load demand, the proposed three-port converter can be operated under two modes. In the battery balance mode (mode 1), MPPT is always operated for the PV port to draw maximum power from the solar panels. Battery port will maintain the power balance by storing the unconsumed solar power during light load condition or providing the power deficit during heavy load condition. The power sharing of the inputs can be represented as:

Pload =P pv-SVC+ P bat-SVC   eqn..   (3.1)

Where Pload is the load demand power, Ppv_SVC is the PV power under solar voltage control (SVC) and Pbat_ SVC is the battery power under SVC. In mode 1, maximum power is drawn from the PV source. Battery may provide or absorb power depending on the load demand. Therefore, Pbat_SVC could be either positive or negative. When the battery charging voltage is higher than the maximum setting, the converter will be switched into battery management mode (mode 2). In mode 2, MPPT will be disabled therefore only part of the solar power is drawn. However, the battery voltage could be controlled to protect the battery from overcharging. The power sharing of the inputs can be represented as:

Pload =Ppv-BVC + Pbat-BVC   eqn..   (3.2)

Where Pbat_BVC is the PV power under battery voltage control (BVC) and Pbat_BVC is the battery charging power under SVC. If the load is increased and the battery voltage is reduced, the converter will be switched to mode 1. The output voltage is always kept at 380V in both modes Operation of the Topological ModesBefore performing the analysis, some assumptions should be made: i) The switches are assumed to be ideal; ii) The magnetizing inductors are large enough so that the current flows through the inductors are constant; iii) The capacitors are large enough so that the voltages across the capacitors are constant. The topological modes over a switching cycle are shown from Fig. 3.1 to Fig. 2.11 and key waveforms of the proposed converter are given in Fig. 3.12

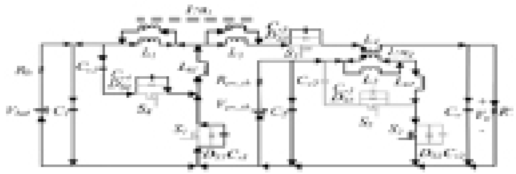

Fig. 3.1 Topological modes of the proposed converter - Interval 1.

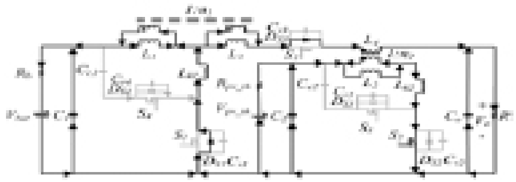

Fig.3.2 Topological modes of the proposed converter- Int-erval 2.

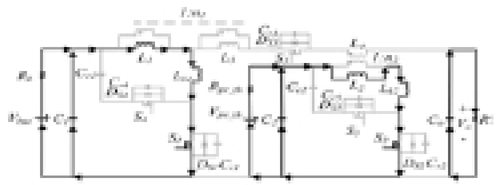

Fig. 3.3 Topological modes of the proposed converter -Interval 3.

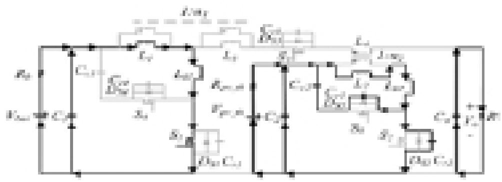

Fig. 3.4 Topological modes of the proposed converter - Interval 4.

Fig. 3.5 Topological modes of the proposed converter- Interval 5.

ISSN No: 2348-4845
International Journal & Magazine of Engineering, Technology, Management and Research
A Peer Reviewed Open Access International Journal

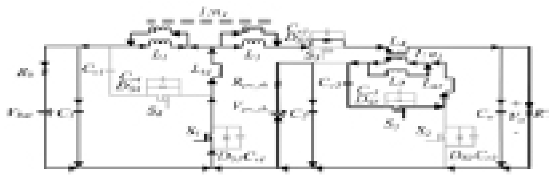

Fig.3.6 Topological modes of the proposed converter - Interval 6.

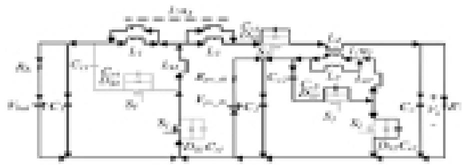

Fig. 3.7 Topological modes of the proposed converter - Interval 7.

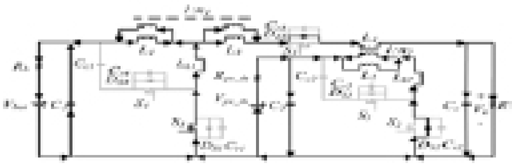

Fig. 3.8 Topological modes of the proposed converter - Interval 8.

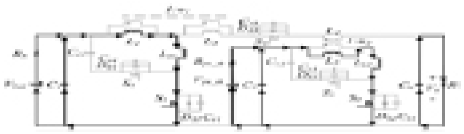

Fig. 3.9 Topological modes of the proposed converter - Interval 9.

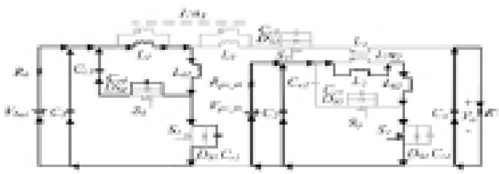

Fig.3.10 Topological modes of the proposed converter - Interval 10.

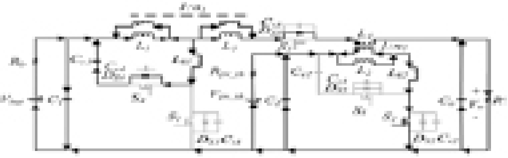

Fig. 3.11 Topological modes of the proposed converter - Interval 11.

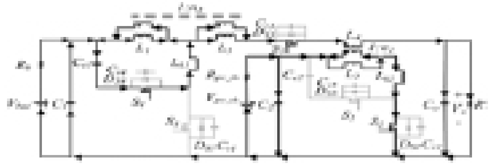

Fig. 3.12 Topological modes of the proposed converter - Interval 12.

Detailed explanation of each interval is given as follows:

Interval 1 [Fig. 3.1, $t_0 \le t < t_1$]: At t0, S1 and auxiliary switches S4 and S5 are turned off while primary switch S2 is turned on. Although S1 is in the off-state, resonant inductor Lk1 resonates with Cr1 and Cr4. In this period, Cr1 is discharged to zero and Cr4 is charged to Vbat+VCc1. For the PV port, S2 is turned on and the current from the PV panels flow through Vpv_th-L2-Lk2-S2 loop. In order to achieve the ZVS feature for S1, the energy stored in resonant inductor Lk1

$$0.5*L_{k1}*[\ i_{LK1}(t_0)]^2 \ge 0.5*(C_{r1}[]C_{r4})*[V_{DS1}(t_0)]^2 \quad \text{eqn.. (3.3)}$$

Interval 2 [Fig. 3.2, $t_1 \le t < t_2$]: This interval starts when vds1 is down to zero. The body diode of S1 is forward biased so that the ZVS condition for S1 is established. The resonant current iLk1 is increased toward zero. L2 is still linearly charged in this period.

Interval 3 [Fig. 3.3, $t_2 \le t < t_3$]: S1 begins to conduct current at t2 and the battery port current follows the path Vbat-L1-Lk1-S1. S2 is also turned on in this interval. Therefore, both L1 and L2 are linearly charged and energy of both input ports is stored in these magnetizing inductors. Auxiliary switches S3, S4, and S5 are all turned off.

Interval 4 [Fig. 3.4, $t_3 \le t < t_4$]: In this interval, S2 starts to be turned off and the auxiliary switch S5 remains in the off-state. However, a resonant circuit formed by Lk2, Cr2, and Cr5 releases the energy stored in Lk2. Resonant capacitor Cr2 is quickly charged to Vpv_th+VCc2 while Cr5 is discharged to zero. In order to achieve the ZVS feature for S5, the energy stored in resonant inductor Lk2 should satisfy the following inequality:

$$0.5*L_{k2}*[\ i_{Lk2}(t_3)]^2 \ge 0.5(C_{r1}[]\ C_{r4})*\ [\ V_{DS5}(t_3)\ ]^2 \quad \text{eqn.. (3.4)}$$

Interval 5 [Fig. 3.5, $t_4 \le t < t_5$]: At t4, vds5 reaches zero and the body diode across the auxiliary switch S5 is turned on. Therefore, a ZVS condition for S5 is

ISSN No: 2348-4845
International Journal & Magazine of Engineering,
Technology, Management and Research
A Peer Reviewed Open Access International Journal

established. Given that the Cr5 is much smaller than CC2, almost all the magnetizing current is recycled to charge the clamp capacitor CC2. Furthermore, VCc2 is considered as a constant value since the capacitance of CC2 is large enough. This interval ends when inductor current iLk2 drops to zero.

Interval 6 [Fig. 3.6, t5≤ t < t6]: At t5, the current of Lk2 is reversed in direction and energy stored in Cc2 is released through the CC2-S5-Lk2-L3 loop. This interval ends when S5 is turned off.

Interval 7 [Fig. 3.7, t6 ≤ t < t7]: Switches S2 and S5 are both in the off-state at t6. A resonant circuit is formed by Lk2, Cr2, and Cr5. During this interval, Cr2 is discharged to zero and Cr5 is charged to Vpv_th+VCc2. To ensure the ZVS switching of S2, the energy stored in Lk2 should be greater than the energy stored in parasitic capacitors Cr2 and Cr5:

$$0.5*L_{K2}*[i_{LK2}(t6)]^2 \geq 0.5*(C_{r1}[]C_{r4})*[V_{DS2}(t6)]^2 \quad \text{eqn.. (3.5)}$$

Interval 8 [Fig. 3.8, t7 ≤ t < t8]: This interval starts when the voltage across Cr2 is zero and the body diode DS2 is turned on. Leakage inductor current iLk2 is linearly increased and the secondary side current of the coupled inductor is increased as well. The main switch S2 should be turned on before iLk2 becomes positive to ensure ZVS operation.

Interval 9 [Fig. 3.9, t8 ≤ t < t9]: The circuit operation of interval 9 is identical to interval 3 since S1 and S2 are turned on in both intervals.

Interval 10 [Fig. 3.10, t9 ≤ t < t10]: At t9, S1 is turned off while S3 and S4 remain in off-state. During this interval, Lk1 will resonant with Cr1 and Cr4 to release the energy trapped in it. Resonant capacitor Cr1 is charged to Vbat+VCc1 while Cr4 is discharged to zero. To achieve the ZVS feature for S4, the energy stored in resonant inductor Lk2 should satisfy the following inequality:

$$0.5*L_{K1}*[i_{LK1}(t9)]^2 \geq 0.5*(C_{r1}[]C_{r4})*[V_{DS1}(t9)]^2 \quad \text{eqn.. (3.6)}$$

Interval 11 [Fig. 3.11, t10 ≤ t < t11]: This interval begins when vds4 drops to zero and the body diode across S4 is turned on. The ZVS condition for S4 is then established. Almost all the magnetizing current is recycled to charge CC1 since Cr4 is much smaller than CC1.

Moreover, VCc1 is considered as a constant value since the capacitance of CC1 is large enough. This interval ends when inductor current iLk1 reaches zero.

Interval 12 [Fig.3.12, t11 ≤ t < t12]: The current flow through Lk1 is reversed in direction at t11, and the energy stored in CC1 is released through the CC1-S4-Lk1-L1 loop. This interval ends when S4 is turned off and the operation of the proposed converter over a switching cycle is complete.

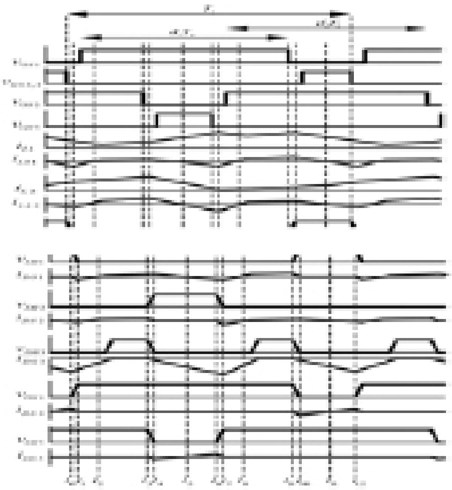

Fig. 3.15 Key waveforms of the proposed converter.
Hardware Circuit and Components

Experimental Setup:

A 200-W laboratory prototype is built and tested under different solar irradiation or load demand as shown in Fig.4.1 Furthermore, the transition of the operation modes and the control strategies are presented. The switches S1 – S4 are implemented with one MOSFET IXFH88N30P (Rds(on) = 0.04 Ω, Coss = 950 pF, TO-247,) S5 is implemented with one MOSFET STW13NK100Z (Rds(on) = 0.56 Ω, Coss = 455 pF, TO-247.) Some other parameters used for the prototype are given in Table I. Again, all the control loops are implemented in a single microcontroller (TMS320F28335).

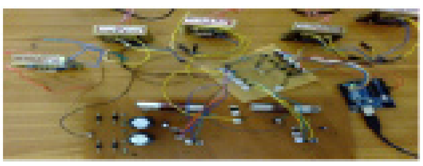

Fig.4.1. Hard ware circuit for the proposed three port converter.

Circuit Parameters

ISSN No: 2348-4845
International Journal & Magazine of Engineering, Technology, Management and Research
A Peer Reviewed Open Access International Journal

Parameter	Value
V_{bat}	48V
V_{pv_mpp} (1000W/m^2)	[illegible]
V_o	380V
P_{pv_max} (1000W/m^2)	300W
P_{load}	300W
f_{sw}	50kHz
[illegible]	[illegible]
[illegible]	[illegible]
[illegible]	[illegible]
[illegible]	470μF
C_o	47μF

Simulation results :

The operation region for the proposed three-port converter is verified as follows: 1) supply the load from each input source independently; 2) share the load between the input sources; 3) the main source (PV) supplies the load and charging the battery at reduced load. In the simulation results, the maximum power rating is set as 300 W (1 p.u). The power Pbat, p.u is limited to-0.3 p.u. since the maximum charging current for the battery is limited in our hardware prototype. In all the figures showing simulation results, the unit of x-axis is sec and y-axis is volt for voltage waveforms and ampere for current waveforms. It is noted that the direction of battery current measurement in operating points A, B and E is opposite to operating points C and D.

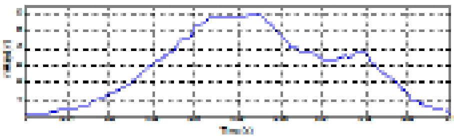

4.2. Simulation wave forms:

a)Solar irradiation voltage:

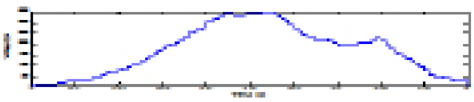

b) Solar output voltage

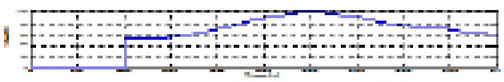

c) Output voltage

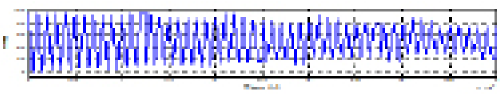

d) Output current

Fig. 4.2 Operating point (A-D): voltage and current waveforms of three ports.

It can be observed from Fig. 4.2 that the load demand is 300 W and is supplied by the battery port at operating point A. The solar irradiation level at this operating point is 0 W/m2. In Fig. 4.2, the voltage and current waveforms for the switches are shown and ZVS switching in the proposed converter for this operating point is verified.

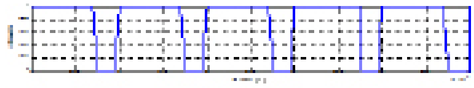

a) Gate pulse s1

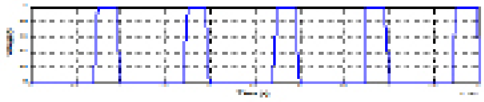

b) Gate pulse s4

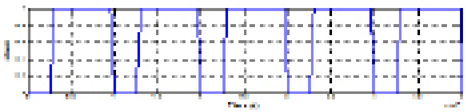

c) Gate pulse s2

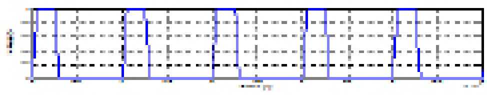

d) Gate pulse s5

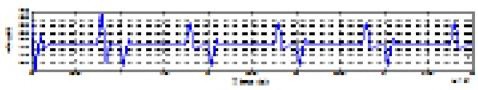

e) Switch across voltage(s1)

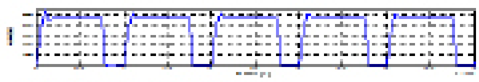

f) switch across current s1

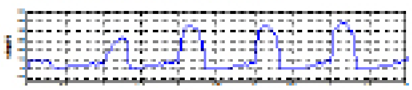

g) Switch across voltage s2

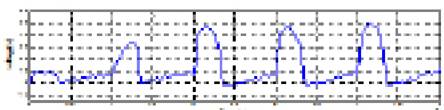

h) Switch across current s2

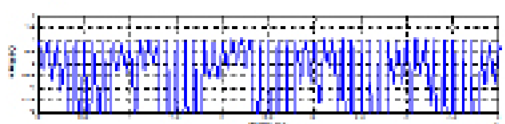

ISSN No: 2348-4845
International Journal & Magazine of Engineering, Technology, Management and Research
A Peer Reviewed Open Access International Journal

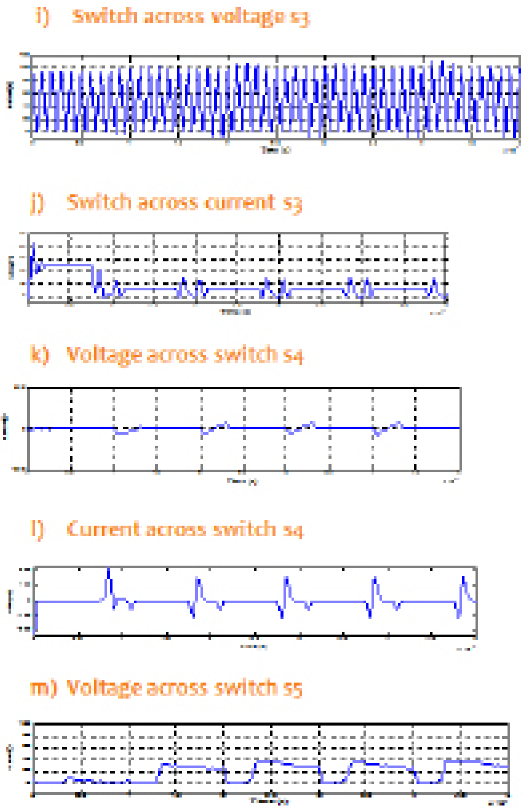

n)Current across switch s5

Fig.4.3 Operating point (a-n): gate pulse, voltage and current waveforms for the switches.

It can be observed from Fig 4.3 that the load is reduced to 105W at operating point D. In addition, the solar irradiation level is decreased to 500W/m2. The PV power is still larger than the load demand at this operating point so the battery will be charged. In Fig. 3.30, the voltage and current waveforms for the switches are shown and ZVS switching in the proposed converter for this operating point is verified.

Conclusion :

This research work focus on development of high step-up PV power conversion. In general, a high step-up PV power system can be established by two-stage or single-stage configuration. Individual research motivation is described at the beginning of the development roadmap of high step-up power electronics converters is described.

Two major issues for high step-up DC-DC converters are indicated: cost and efficiency. The DC-AC inverters that are proposed for high step-up applications are also introduced. Connecting the high step-up DC-DC converters to a DC-AC central inverter is the most common configuration in industrial applications. A microgrid built with distributed energy sources is studied as an example of renewable energy systems.

The proposed switching strategy only needs to control two duty ratios in different operation modes. The charging/discharging operation of battery could be achieved without changing the operation mode. The output voltage is always regulated at 380 V. The control method of battery port could be modified for the grid-connected applications.

REFERENCES:

[1] E. Figueres, G. Garcera, J. Sandia, F. Gonzalez-Espin, and J. C. Rubio, “ Sensitivity study of the dynamics of three-phase photovoltaic inverters with an LCL grid filter, ”IEEE Trans. Ind. Electron., vol. 56, no. 3, pp. 706–717, Mar. 2009.

[2] Q. Li and P. Wolfs, “A review of the single phase photovoltaic module integrated converter topologies with three different dc link configurations,” IEEE Trans. Power Electron., vol. 23, no. 3, pp. 1320–1333, May 2008.

[3] IMS Research, 2011. Available: http://www.pv-tech.org/news/1778, January 17, 2011.

[4] German Advisory Council on Global Change WBGU Berlin 2003; Renewable Energy Policy Network for the 21st Century, Renewables, Global Status Report 2006.

[5] (2003) Trends in Photovoltaic Applications. Survey Report of Selected IEA Countries Between 1992 and 2002. International Energy Agency Photovoltaic Power Systems, IEA PVPS T1-12:2003.

[6] S. B. Kjaer, J. K. Pedersen, and F. Blaabjerg “A Review of Single-Phase Grid-Connected Inverters for Photovoltaic Modules,” IEEE Trans. Ind. Appl., vol. 41, no. 5,pp. 1292-1306, Sept/Oct. 2005..

[7] J. Selvaraj and N. A. Rahim, "Multilevel inverter for grid-connected PV system employing digital PI controller," IEEE Trans. Ind. Electron., vol. 56, no. 1, pp. 149–158, Jan. 2009.

[8] V. Scarpa, S. Buso, and G. Spiazzi, "Low-complexity MPPT technique exploiting the PV module MPP locus characterization," IEEE Trans. Ind. Electron., vol. 56, no. 5, pp.1531–1538, May 2009.

[9] T. Shimizu, O. Hashimoto, and G. Kimura, "A novel high-performance utility interactive photovoltaic inverter system," IEEE Trans. Power Electron., vol. 18, no. 2, pp. 704–711, Mar. 2003.

[10] W. Li and X. He, "Review of nonisolated high-step-up DC/DC converters in photovoltaic grid-connected applications," IEEE Trans. Ind. Electron., vol. 58, no. 4, pp.1239-1250, Apr. 2011.

[11]R.W. Erickson and D. Masksimovic, Fundamentals of Power Electronics. 2nd Ed.Norwell, MA: Kluwer, pp. 40–56.

[12]K.M. Smith and K. M.Smedley, "Properties and synthesis of passive lossless soft switching PWM converters," IEEE Trans. Power Electron., vol. 14, no. 5, pp. 890–899, Sep. 1999.

[13] M. M. Jovanovic and Y. Jang, "State-of-the-art, single-phase, active power-factorcorrection technique for high-power applications— An overview," IEEE Trans. Power Electron, vol. 52, no. 3, pp. 701–708, Jun. 2005.

[14] N. P. Papanikolaou and E. C. Tatakis, "Active voltage clamp in flyback converters operating in CCM mode under wide load variation," IEEE Trans Ind. Electron, vol. 51, no. 3, pp. 632–640, Jun. 2004.